JOURNAL OF SPACECRAFT AND ROCKETS
Vol. 45, No. 6, November–December 2008

Receptivity of a Hypersonic Flat-Plate Boundary Layer to Three-Dimensional Surface Roughness

Xiaowen Wang* and Xiaolin Zhong†
University of California, Los Angeles, Los Angeles, California 90095

DOI: 10.2514/1.37766

The laminar–turbulent transition of hypersonic boundary layers has a significant effect on drag calculation and aerothermal design of hypersonic vehicles. Recent research has shown that one possible explanation to roughness-induced bypass transition is transient growth theory. However, it is not known how to generate the optimal disturbances computed by transient growth theory. Furthermore, there has not been any direct numerical simulation study on transient growth in hypersonic boundary layers. The objectives of this paper are to study the receptivity of a Mach 5.92 flow over a flat plate to three-dimensional surface roughness and the effect of spanwise wave number on the receptivity. Steady base flow is computed by solving compressible Navier–Stokes equations with a combination of a fifth-order shock-fitting method and a second-order total variation diminishing scheme. In receptivity simulations, small surface roughness is introduced on the plate. The numerical results show that counter-rotating streamwise vortices and transient growth are induced by surface roughness, however, transient growth is generally weak due to the small height of roughness. For the six cases considered, surface roughness with the spanwise wave number being 0.0101 has the strongest excitation of transient growth.

I. Introduction

THE laminar–turbulent transition of hypersonic boundary-layer flows has a significant effect on the drag calculation and aerothermal design of hypersonic vehicles. To predict and control boundary-layer transition, extensive studies have been carried out to investigate transition mechanisms [1–5]. It is recognized that the transition process of a boundary-layer flow strongly depends on the amplitude level of environmental perturbations [6], which is schematically shown in Fig. 1. According to Reshotko's analysis [7], only the first three paths had relevance to external flows. In an environment of small amplitude perturbations, transition of the boundary-layer flow over a smooth surface generally consists of three steps (path 1): 1) receptivity process during which small amplitude environmental disturbances enter the boundary layer and excite boundary-layer wave modes; 2) linear development or growth of unstable boundary-layer wave modes which can be predicted by solving the eigenproblem of the homogeneous linearized stability equations; 3) boundary-layer transition caused by nonlinear breakdown and three-dimensional effects when the unstable wave modes reach certain amplitudes. For high-amplitude perturbations, transient growth provides a higher initial amplitude to eigenmode growth (path 2). On a nonsmooth surface with stationary roughness elements, the strong transient growth of boundary-layer wave modes may directly lead to transition (path 3). In the current paper, only small surface roughness is considered. The undergoing path in this particular case configuration is path 3. However, the transient growth is too weak to lead to transition.

The study of receptivity process is of critical importance to the prediction of transition because it provides initial conditions of amplitude, frequency, and phase angle for boundary-layer wave modes [8]. Recently, theoretical, experimental, and numerical simulation studies on the receptivity of two- and three-dimensional boundary layers have been carried out by many researchers [5,9–12].

Mack [2] was the first to carry out extensive computations on the linear stability characteristics of compressible boundary layers. He used compressible linear stability theory (LST) to calculate the amplitude ratio (A/A_0) of constant-frequency disturbances as a function of Reynolds number, where A and A_0 were local disturbance amplitude and initial disturbance amplitude. The transition Reynolds number was determined by an amplitude-ratio criterion. For a cooled-wall flat-plate supersonic boundary layer, it was found that calculated transition Reynolds number increased much faster than the experimental measurements. Such results indicated that LST alone was insufficient to accurately determine the transition Reynolds number. It was necessary to consider the properties of the environmental disturbances and the initial excitations of boundary-layer wave modes. By solving the nonlinear parabolized stability equations (PSE), Bertolotti [13] studied the amplification of vortices over a plate generated by surface roughness, blowing suction, or both. The results showed that the growth of vorticity could be much larger with the presence of both wall inhomogeneities. Choudhari [14] studied the roughness-induced generation of stationary and nonstationary vortices in three-dimensional boundary layers over a sweep wing, where nonstationary vortices were induced with the presence of freestream acoustic disturbances. The effects of acoustic-wave orientation and different types of roughness geometries were considered. It was found that maximum receptivity occurred when the velocity fluctuation of an acoustic disturbance was aligned with the wave number vector of a nonstationary vortex mode. Hanifi et al. [15] investigated temporal transient growth phenomena of boundary-layer flows at a series of Mach numbers from 0.1 to 4.5 using the spectral collocation method. They found that maximum transient growth increased with Mach number and could be scaled with Re^2, where Re is the Reynolds number defined by using freestream flow variables and Blasius boundary-layer thickness $(\sqrt{\mu^*_\infty x/\rho^*_\infty u^*_\infty})$. In addition, the time at which the maximum transient growth was reached could be scaled with Re. Andersson et al. [16] numerically calculated the maximum transient growth for steady disturbances and concluded that optimal disturbances consisted of streamwise vortices. They also found that maximum transient growth scaled linearly with the distance from the leading edge. Recently, Tumin [17] solved the receptivity problem of compressible boundary layers to three-dimensional wall perturbations by using a biorthogonal eigenfunction system. In case of receptivity to surface roughness, a small-height hump was

Presented as Paper 503 at the 46th AIAA Aerospace Sciences Meeting and Exhibit, Reno, NV, 7–10 January 2008; received 27 March 2008; revision received 17 June 2008; accepted for publication 1 July 2008. Copyright © 2008 by the American Institute of Aeronautics and Astronautics, Inc. All rights reserved. Copies of this paper may be made for personal or internal use, on condition that the copier pay the $10.00 per-copy fee to the Copyright Clearance Center, Inc., 222 Rosewood Drive, Danvers, MA 01923; include the code 0022-4650/08 $10.00 in correspondence with the CCC.

*Postdoctoral Researcher, Mechanical and Aerospace Engineering Department; xiaowen@seas.ucla.edu. AIAA Member.

†Professor, Mechanical and Aerospace Engineering Department; xiaolin@seas.ucla.edu. AIAA Associate Fellow.

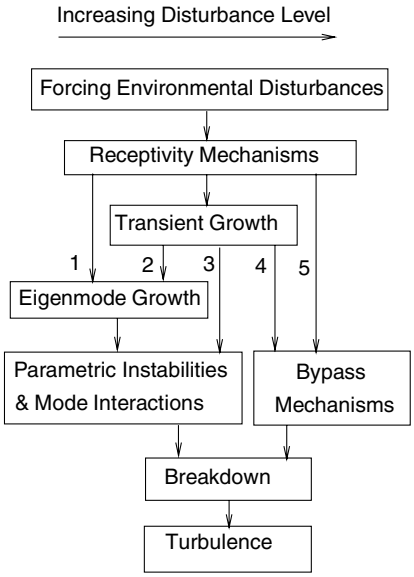

Fig. 1 Paths of boundary-layer transition process with respect to disturbance amplitude [6].

considered. The results showed that there were counter-rotating streamwise vortices, streaks at both sides of the hump, and a wake region downstream from the hump. Outside of the boundary layer, there existed large amplitude perturbations near the Mach waves generated by the hump.

Because of the difficulties in carrying out supersonic and hypersonic receptivity experiments, very few experimental studies on receptivity, stability, and transient growth have been reported. Kendall [3] experimentally studied the origin and growth of natural fluctuations in zero pressure-gradient boundary layers at several Mach numbers ranging from 1.6 to 8.5. Substantial growths of flow fluctuations were observed within the laminar boundary layer in the early region where the boundary layer was predicted to be linearly stable. These fluctuations were related to the acoustic noise for hypersonic flows. The growth rates of these fluctuations in the region downstream of the initial growth were in a reasonable agreement with the LST results of Mack [2]. Maslov and Semenov [18] experimentally investigated the receptivity of a supersonic boundary layer to artificial acoustic waves by using two parallel flat plates. The acoustic waves generated by an electric discharge system on the lower plate radiated into the external flow and penetrated into the boundary layer of the upper plate as freestream acoustic disturbances. It was found that the acoustic disturbances were converted into boundary-layer wave modes most efficiently at the leading edge and in the neighborhood of lower and upper branches of the neutral curve. A similar experiment was carried out at a Mach 5.92 flow by Maslov et al. [5] to study the leading-edge receptivity of the hypersonic boundary layer. It was observed that Tollmien–Schlichting waves were generated by the acoustic waves impinging on the leading edge. They also found that the receptivity coefficients depended on wave inclination angles. White [19] investigated the transient growth of a flat-plate boundary layer to controlled stationary disturbances generated by using spanwise roughness array. The results showed quantitative differences between experimental measurements and theoretical predictions, which did indicate that realistic stationary disturbances could exhibit significant nonoptimal behavior. White and Ergin [20] further studied the receptivity and transient growth of a Blasius boundary layer to roughness-induced disturbances, where the initial disturbances were generated by a spanwise array of roughness elements. In experiments, detailed information on the disturbances and the transient growth was measured using hot-wire instruments. The results indicated that energy associated with the roughness-induced disturbances scaled with the roughness-based Reynolds number. Fransson and Brandt [21] experimentally and theoretically investigated the transient growth of stationary streamwise streaks in a flat-plate boundary layer. The stable laminar streaks were periodic in the spanwise direction and were generated by a spanwise periodic array of small cylindrical roughness elements. The results showed that the maximum transient growth was mainly determined by the height of roughness elements. Recently, White et al. [22] investigated the effects of the amplitude and diameter of cylindrical roughness elements on transient growth features. Their experimental results showed that energy of stationary disturbances varied as Re_k^2, the square of roughness-based Reynolds number, and the qualitative nature of transient growth strongly depended on the roughness diameter.

Recently, there are many numerical simulation studies in supersonic and hypersonic boundary-layer receptivity. Bottaro and Zebib [23] numerically investigated the formation and growth of spatial Görtler vortices induced by wall roughness. In all naturally developing cases, the average spanwise wavelengths of vortices were close to those of optimal disturbances predicted by LST. Collis and Lele [24] numerically investigated the formation of stationary crossflow vortices in a three-dimensional boundary layer due to surface roughness near the leading edge of a swept wing. The results showed that convex surface curvature enhanced receptivity, whereas nonparallel effects strongly reduced the initial amplitude of stationary crossflow vortices. Malik et al. [4] investigated the responses of a Mach 8 flow over a sharp wedge of a half-angle of 5.3 deg to three types of external forcing: a planar freestream acoustic wave, a narrow acoustic beam enforced on the bow shock near the leading edge, and a blowing-suction slot on the wedge surface. They concluded that these three types of forcing eventually result in the same type of instability waves in the boundary layer. Zhong [25] studied the acoustic receptivity of a hypersonic flow over a parabola by solving full Navier–Stokes equations. It was concluded that the generations of boundary-layer wave modes were mainly owing to the interaction of the boundary layer with the transmitted acoustic waves instead of entropy and vorticity waves. In a series of papers, Ma and Zhong [11,12,26] studied the receptivity of a supersonic boundary layer to various freestream disturbances by a combination of numerical simulation and linear stability theory. It was found that, in addition to the conventional first and second Mack modes, there existed a family of stable modes that played an important role in the excitation of unstable modes. Egorov et al. [27] simulated unsteady two-dimensional flows relevant to receptivity of supersonic and hypersonic boundary layers by using a total variation diminishing (TVD) scheme. For small forcing amplitudes, the second-mode growth rates obtained by numerical simulation agreed well with those predicted by LST, including the nonparallel effects. The results of their simulations showed a nonlinear saturation of fundamental harmonic and rapid growth of higher harmonics. Fischer and Choudhari [28,29] examined the roughness-induced transient growth in a laminar boundary layer due to a spanwise periodic array of circular disks at the surface. The effects of roughness height, size, and shape on the transient growth were also explored. Their numerical simulation results indicated that energy levels of the dominant stationary disturbances were consistent with the Re_k^2 scaling of White et al. [22]. Spontaneous vortex shedding behind the roughness array was identified for sufficiently large roughness heights. Wang and Zhong [30] studied the receptivity of the same flow as in Malik et al.'s [4] investigation to periodic blowing-suction disturbances introduced in a narrow region on the wall. The effects of frequency, location, and length of the blowing-suction actuator on the receptivity process were also investigated based on a series of numerical simulations. The numerical results showed that mode F, mode S, and acoustic modes were excited by the blowing-suction disturbances. Far downstream of the forcing region, mode S became the dominant mode in the boundary layer. All cases of numerical simulations consistently showed that the synchronization point of mode F and mode S played an important role in the excitation of mode S by wall blowing-suction. A concurrent theoretical study had been carried out by Tumin et al. [10] to compare the theoretical and numerical results of receptivity coefficients and to analyze the receptivity characteristics. The perturbation flowfield downstream of

the blowing-suction actuator was decomposed into boundary-layer wave modes with the help of the biorthogonal eigenfunction system. It was found that there was a good agreement between normal-mode amplitudes calculated with the help of the theoretical receptivity model and those obtained by projecting the numerical results onto the normal modes.

Recent research has shown that one possible explanation to roughness-induced bypass transition is the transient growth theory pioneered by Reshotko and Tumin [31]. According to their theory, transient growth arose through the coupling between slightly damped Orr–Sommerfeld and Squire modes. They defined an energy norm in the form of a production of density and squared velocity, where the roughness-induced velocity is assumed proportional to the roughness height. The energy norm at transition was related to the initial energy norm through a transient growth factor. As a result, a correlated transient growth factor could be used to predict the transition location. Furthermore, the optimal disturbance was defined as the disturbance to achieve the maximum energy growth at the specific downstream coordinate. However, it is noticed that there has not been any direct numerical simulation study on transient growth in hypersonic boundary layers. Furthermore, it is not known how the optimal disturbances computed by the transient growth theory are generated by surface roughness. These are important issues related to the receptivity of transient growth, which need to be resolved. In this paper, the receptivity of a hypersonic flat-plate boundary layer to three-dimensional surface roughness is studied by a series of numerical simulations. The freestream flow conditions are the same as those of Maslov et al.'s [5] leading-edge receptivity experiments. Steady base flow is first computed by solving compressible Navier–Stokes equations with a combination of a fifth-order shock-fitting method and a second-order TVD scheme. The accuracy of the numerical steady base flow is validated by comparisons with the theoretical self-similar boundary-layer solution and Maslov et al.'s experimental measurements. In receptivity simulations, small surface roughness, periodic in the spanwise direction, is introduced on the flat plate. The subsequent responses of the hypersonic boundary layer are simulated by solving three-dimensional Navier–Stokes equations with a fifth-order shock-fitting method and a Fourier collocation method. Because of the small height of roughness element, boundary conditions of temperature and velocities on the rough surface are transferred to the original smooth surface by linear extrapolation. The effect of spanwise wave number on the receptivity is studied by considering six cases of receptivity simulations.

II. Governing Equations and Numerical Methods

In the current numerical study, a Mach 5.92 flow over a flat plate, as shown in Fig. 2, is considered. The flow is assumed to be thermally and calorically perfect. The governing equations for the simulation are the full Navier–Stokes equations in the conservative form, that is,

$$\frac{\partial \mathbf{U}^*}{\partial t^*} + \frac{\partial}{\partial x_1^*}(\mathbf{F}_{1i}^* + \mathbf{F}_{1v}^*) + \frac{\partial}{\partial x_2^*}(\mathbf{F}_{2i}^* + \mathbf{F}_{2v}^*) + \frac{\partial}{\partial x_3^*}(\mathbf{F}_{3i}^* + \mathbf{F}_{3v}^*) = 0 \tag{1}$$

where the superscript "$*$" represents dimensional variables. $\mathbf{U}^*$ is a vector containing the conservative variables of mass, momentum, and energy, that is,

$$\mathbf{U}^* = \{\rho^*, \rho^* u_1^*, \rho^* u_2^*, \rho^* u_3^*, e^*\} \tag{2}$$

The flux vector in Eq. (1) is divided into its inviscid and viscous components, because the two components are discretized with different schemes. The components $\mathbf{F}_{1i}^*$, $\mathbf{F}_{2i}^*$, $\mathbf{F}_{3i}^*$ are inviscid flux vectors, whereas $\mathbf{F}_{1v}^*$, $\mathbf{F}_{2v}^*$, and $\mathbf{F}_{3v}^*$ are viscous flux vectors. The flux vectors can be expressed as

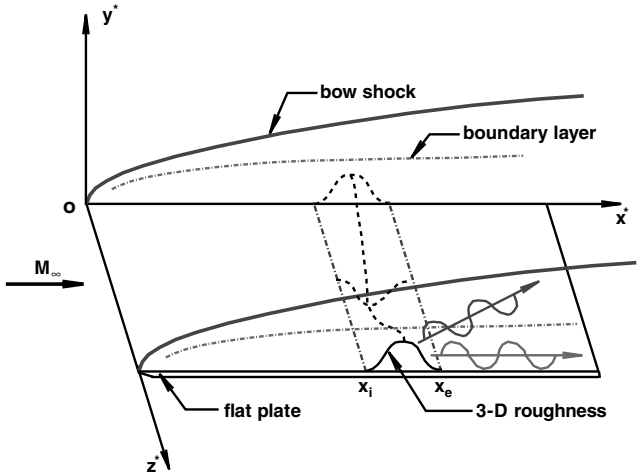

Fig. 2 Schematic of the receptivity of the Mach 5.92 flow to three-dimensional surface roughness.

$$\mathbf{F}_{ji}^* = \begin{bmatrix} \rho^* u_j^* \\ \rho^* u_1^* u_j^* + p^* \delta_{1j} \\ \rho^* u_2^* u_j^* + p^* \delta_{2j} \\ \rho^* u_3^* u_j^* + p^* \delta_{3j} \\ u_j^*(e^* + p^*) \end{bmatrix}, \quad \mathbf{F}_{jv}^* = \begin{bmatrix} 0 \\ -\tau_{1j}^* \\ -\tau_{2j}^* \\ -\tau_{3j}^* \\ -\tau_{1j}^* u_1^* - \tau_{2j}^* u_2^* - \tau_{3j}^* u_3^* + k^* \frac{\partial T^*}{\partial x_j^*} \end{bmatrix} \tag{3}$$

with $j \in \{1, 2, 3\}$. In Eq. (3), δ_{ij} $(i = 1, 2, 3)$ is the Kronecker delta function. In the perfect gas assumption, pressure and energy are given by

$$p^* = \rho^* R^* T^* \tag{4}$$

$$e^* = \rho^* c_v^* T^* + \frac{\rho^*}{2}(u_1^{*2} + u_2^{*2} + u_3^{*2}) \tag{5}$$

where c_v^* is the specific heat at constant volume. For compressible Newtonian flow, the viscous stress tensor can be written as

$$\tau_{ij}^* = \mu^* \left(\frac{\partial u_i^*}{\partial x_j^*} + \frac{\partial u_j^*}{\partial x_i^*} \right) - \frac{2}{3} \mu^* \left(\frac{\partial u_1^*}{\partial x_1^*} + \frac{\partial u_2^*}{\partial x_2^*} + \frac{\partial u_3^*}{\partial x_3^*} \right) \delta_{ij} \tag{6}$$

with $i, j \in \{1, 2, 3\}$. In the simulation, the viscosity coefficient μ^* and the heat conductivity coefficient k^* are calculated using Sutherland's law together with a constant Prandtl number Pr. They are both functions of temperature only:

$$\mu^* = \mu_r^* \left(\frac{T^*}{T_r^*} \right)^{3/2} \frac{T_r^* + T_s^*}{T^* + T_s^*} \tag{7}$$

$$k^* = \frac{\mu^* c_p^*}{Pr} \tag{8}$$

where $\mu_r^* = 1.7894 \times 10^{-5}$ Ns/m^2, $T_r^* = 288.0$ K, $T_s^* = 110.33$ K, and c_p^* is the specific heat at constant pressure. In this paper, the dimensional flow variables are nondimensionalized by freestream parameters. Specifically, density ρ^*, temperature T^*, velocities u_1^*, u_2^*, u_3^*, and pressure p^* are nondimensionalized by ρ_∞^*, T_∞^*, u_∞^*, and $\rho_\infty^* u_\infty^{*2}$. Furthermore, x_1^* and x_3^* are nondimensionalized by unit length in meters, whereas x_2^* is nondimensionalized by Blasius boundary-layer thickness, $\sqrt{\mu_\infty^* x_1^* / \rho_\infty^* u_\infty^*}$. Referring to the coordinate system shown in Fig. 2, x_1^*, x_2^*, and x_3^* are x^*, y^*, and z^*, respectively. The three variables u_1^*, u_2^*, and u_3^* are velocities in streamwise, wall-normal, and spanwise directions.

The high-order shock-fitting finite difference method of Zhong [32] is used to solve the governing equations in a domain bounded by the bow shock and the flat plate. In other words, the bow shock is treated as a boundary of the computational domain. The

Rankine–Hugoniot relation across the shock and a characteristic compatibility relation coming from the downstream flowfield are combined to solve the flow variables behind the shock. The shock-fitting method makes it possible for the Navier-Stokes equations to be spatially discretized by high-order finite difference methods. Specifically, a fifth-order upwind scheme is used to discretize the inviscid flux derivatives. Meanwhile, a sixth-order central scheme is used to discretize the viscous flux derivatives. For three-dimensional simulations, flux derivatives of $\mathbf{F}^*_{3i}$ and $\mathbf{F}^*_{3v}$ in the spanwise direction are calculated by the Fourier collocation method to achieve high accuracy. By using the shock-fitting method, the interaction between the bow shock and perturbations induced by wall disturbances is solved as a part of the solution, with the position and velocity of the shock front being taken as dependent flow variables. In the leading-edge region, there exists a singular point at the tip of the flat plate that introduces numerical instability if the fifth-order shock-fitting method is used to simulate the flow. Therefore, the computational domain for the shock-fitting simulation starts from a very short distance downstream of the leading edge. A second-order TVD scheme used by Zhong and Lee [33] is used to simulate the steady base flow in a small region including the leading edge to supply inlet conditions for the shock-fitting simulation. For receptivity simulations, three-dimensional small-scale roughness elements are introduced in a downstream region where the shock-fitting method is used.

The same numerical method has been used by Ma and Zhong in their receptivity studies of supersonic and hypersonic boundary layers over a flat plate and a sharp wedge to various freestream disturbances [11,12,26,34]. The good agreement between numerical and LST results indicates that the high-order shock-fitting finite difference method is accurate to simulate the receptivity problems of high-speed boundary-layer flows. The numerical method has also been validated in the theoretical study and comparison with numerical simulation by Tumin et al. [35]. The numerical perturbation field downstream of the blowing-suction actuator is decomposed into boundary-layer wave modes with the help of the biorthogonal eigenfunction system. The filtered-out amplitudes of mode S and mode F agree well with the theoretical solutions of the linear receptivity problem. The Fourier collocation method has been tested by Zhong [36] to study the receptivity of a Mach 6 flow over a flared cone to freestream disturbances. The numerical results are compared with published experiment results. It is found that the steady base flow solutions agree very well with the experiment results. The wave numbers and growth rates of numerical solutions are reasonably similar to the LST results.

III. Flow Conditions and Boundary Condition Transfer

Freestream flow conditions of the currently studied flow are the same as those of Maslov et al.'s experiment [5], that is,

$$M_\infty = 5.92, \qquad T^*_\infty = 48.69\ \text{K}, \qquad p^*_\infty = 742.76\ \text{Pa},$$
$$Pr = 0.72, \qquad Re^*_\infty = 13 \times 10^6/\text{m}$$

The dimensional streamwise coordinate x^*, as shown in Fig. 2, can be converted to the local Reynolds number by

$$Re_x = Re^*_\infty x^* \tag{9}$$

where Re^*_∞ is the unit Reynolds number defined as

$$Re^*_\infty = \rho^*_\infty u^*_\infty / \mu^*_\infty \tag{10}$$

In LST studies of boundary-layer flows, the Reynolds number based on Blasius boundary-layer thickness L^* is generally used. They are expressed as

$$Re = \frac{\rho^*_\infty u^*_\infty L^*}{\mu^*_\infty}, \qquad L^* = \sqrt{\frac{\mu^*_\infty x^*}{\rho^*_\infty u^*_\infty}} \tag{11}$$

Hence, the relation between Re and local Reynolds number Re_x is given by

$$Re = \sqrt{Re_x} \tag{12}$$

For the simulation of base flow, the wall is adiabatic, and the physical boundary condition of velocity on the flat plate is the nonslip condition. When small surface roughness is introduced on the flat plate, boundary conditions of temperature and velocities on the rough surface are transferred to the original smooth surface by linear extrapolation due to the small height of the roughness element. Figure 3 schematically shows the linear boundary condition transfer of streamwise velocity, where the bold arrows on the undisturbed surface stand for the streamwise velocity boundary conditions for points A and B on original smooth surface. Therefore, the computational domain and grid structure of receptivity simulation are the same as those of base flow simulation. In the smooth region, the adiabatic thermal condition and nonslip condition are used, because the flow in receptivity simulation is still steady flow. Inlet conditions are specified, whereas high-order extrapolation is used for outlet conditions because the flow is hypersonic at the exit boundary except for a small region near the flat plate.

Because of the existence of small roughness, the wall surface changes from $y^* = 0$ to $y^* = \epsilon \hbar^*(x^*, z^*)$, where $y^* = 0$ stands for the original smooth surface. The function $\hbar^*(x^*, z^*)$ represents the profile of roughness elements. The parameter ϵ is used to adjust the height. The physical nonslip conditions of velocity on the rough surface are

$$\begin{cases} u^*(x^*, \epsilon\hbar^*(x^*, z^*), z^*) = 0 \\ v^*(x^*, \epsilon\hbar^*(x^*, z^*), z^*) = 0 \\ w^*(x^*, \epsilon\hbar^*(x^*, z^*), z^*) = 0 \end{cases} \tag{13}$$

Under the assumption of small-height roughness elements, boundary conditions on the rough wall can be transferred to the original smooth surface by linear extrapolation, that is,

$$\begin{cases} u^*(x^*, 0, z^*) = -\epsilon\hbar^*(x^*, z^*) \frac{\partial u^*}{\partial y^*}|_{y^*=0} \\ v^*(x^*, 0, z^*) = -\epsilon\hbar^*(x^*, z^*) \frac{\partial v^*}{\partial y^*}|_{y^*=0} \\ w^*(x^*, 0, z^*) = -\epsilon\hbar^*(x^*, z^*) \frac{\partial w^*}{\partial y^*}|_{y^*=0} \end{cases} \tag{14}$$

From our previous study [37], it was found that the roughness element on an adiabatic flat plate was more efficient in the excitations of streamwise vortices and transient growth. Therefore, the adiabatic temperature condition is used on the rough surface, which is expressed as

$$\frac{\partial T^*(x^*, \epsilon\hbar^*(x^*, z^*), z^*)}{\partial y^*} = 0 \tag{15}$$

Similarly, the temperature condition can be transferred to the original smooth surface as follows:

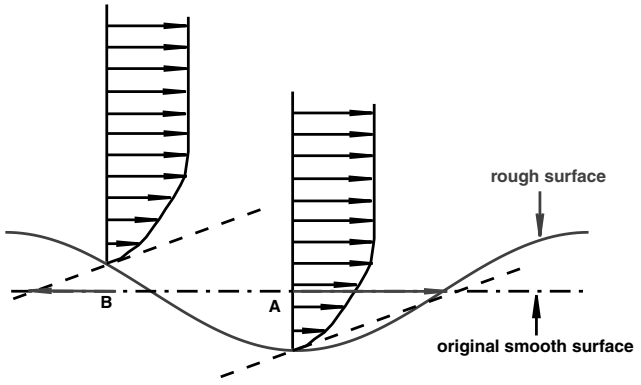

Fig. 3 Schematic of linear boundary condition transfer of streamwise velocity for points A and B on original smooth surface.

$$\frac{\partial T^*(x^*,0,z^*)}{\partial y^*} = -\epsilon\hbar^*(x^*,z^*)\left.\frac{\partial^2 T^*}{\partial y^{*2}}\right|_{y^*=0} \tag{16}$$

In Eqs. (14) and (16), all derivatives on the right-hand side of the equations are calculated from the base flow.

With the linear extrapolations of velocities and temperature, the authors still use the original grids for receptivity simulations. This treatment is widely used in theoretical analysis and numerical simulations for small surface roughness. In transient growth theory, Reshotko and Tumin [31] assumed that the roughness-induced velocity is proportional to the roughness height. Recently, Tumin [17] solved the receptivity problem of compressible boundary layers to three-dimensional wall perturbations by using the biorthogonal eigenfunction system. In his analysis, linear extrapolation of velocity was used to model the hump.

For the roughness elements considered in the current paper, the function of $\hbar^*(x^*, z^*)$ is defined as

$$\hbar^*(x^*,z^*) = \hbar^*(l)\cos(\beta^* z^*) \tag{17}$$

where β^* is the spanwise wave number. The function $\hbar^*(l)$ and the variable l are defined as

$$\hbar^*(l) = (20.25l_4^5 - 35.4375l_4^4 + 15.1875l_4^2)/2.45688 \tag{18}$$

$$l = 0.620287 \times \begin{cases} 2(x^* - x_i^*)/(x_e^* - x_i^*) & \text{if } x^* \le 4.28125 \text{ mm} \\ 2(x_e^* - x^*)/(x_e^* - x_i^*) & \text{if } x^* > 4.28125 \text{ mm} \end{cases} \tag{19}$$

The coordinates of the leading and trailing edges of the roughness elements in the streamwise direction x_i^* and x_e^* are equal to 3.3125 and 5.25 mm, corresponding to $Re = 216.31$ and $Re = 272.32$, respectively. The constant 2.45688 is the value of $\hbar^*(l)$ at $l = 0.620287$, which is used to normalize the profile function.

IV. Results and Discussions

A. Steady Base Flow

Steady base flow over the flat plate is first computed by solving the compressible Navier–Stokes equations with a combination of a fifth-order shock-fitting finite difference method and a second-order TVD scheme. In the leading-edge region, there exists a singular point at the tip of the flat plate that will introduce numerical instability if the fifth-order shock-fitting method is used to simulate the flow. A second-order TVD scheme used by Zhong and Lee [33] is applied to simulate the steady base flow in a small region including the leading edge. The computational domain for the fifth-order shock-fitting method starts at $x^* = 0.0025$ m and ends at $x^* = 0.879$ m, corresponding to $Re = 180.28$ and $Re = 3380.38$, respectively. In actual shock-fitting simulations, the computational domain is divided into 19 zones with a total of 3746 grid points in the streamwise direction. The number of grid points in the wall-normal direction is 121 before the position of $x^* = 0.309$ m, and 176 after that position. Forty-one points are used in the overlap region between two neighboring zones, which is proved to be sufficient to make the solution accurate and smooth within the whole domain. An exponential stretching function is used in the wall-normal direction to cluster more points inside the boundary layer. On the other hand, the grid points are uniformly distributed in the streamwise direction. The spatial convergence of the results based on this grid structure has been evaluated by grid refinement studies to ensure the grid independence of the fifth-order shock-fitting simulations.

For shock-fitting simulation in the first zone, the inlet conditions are obtained from the results of the second-order TVD shock-capturing scheme, which is used to simulate the steady base flow in a small region including the leading edge. For other zones, inlet conditions are interpolated from the results of the previous zone. The computational domain for the second-order TVD scheme starts at $x^* = -0.0005$ m and ends at $x^* = 0.0035$ m ($Re = 213.31$). The combination of the fifth-order shock-fitting method and second-order TVD scheme has also been validated in cases of supersonic and hypersonic steady base flows by Ma and Zhong [38] and Wang and Zhong [30].

Figure 4 shows the pressure contours of the steady base flow simulated by the fifth-order shock-fitting finite difference method. The upper boundary of the flowfield represents the bow shock induced by the displacement thickness of the boundary layer. The lower boundary is the surface of the flat plate. The left inlet of the flowfield starts at $x^* = 0.0025$ m, where the shock has very small, but nonzero, height. A part of the pressure field from $x^* = 0.03$ m to $x^* = 0.08$ m ($Re = 624.50$ to $Re = 1019.80$) is amplified to clearly show the pressure contours within the boundary layer. It is noticed that pressure is approximately constant across the boundary layer and along the Mach lines, which is consistent with the theories of boundary-layer flow and inviscid supersonic aerodynamics. At a fixed location of constant x^*, pressure behind the shock is higher than that on the flat plate due to the existence of the bow shock. More results of the two-dimensional steady base flow can be found in our previous papers [37,39].

To validate the accuracy of numerical simulation, the steady base flow simulated by the fifth-order shock-fitting method is compared with the theoretical self-similar boundary-layer solution and Maslov et al.'s [5] experimental measurements. Figure 5 shows the distributions of dimensionless streamwise velocity across the

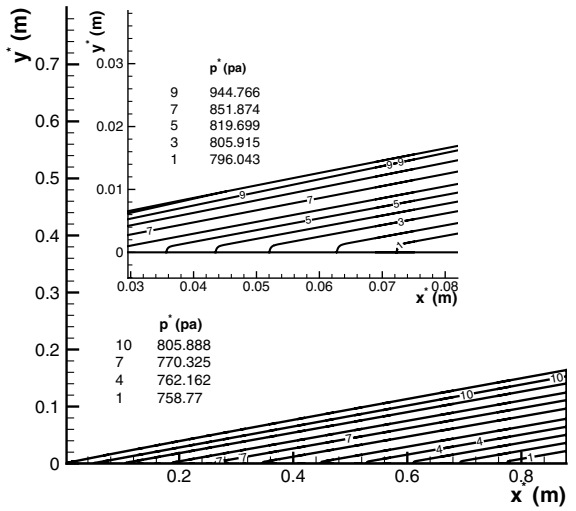

Fig. 4 Pressure contours of the base flow simulated by the fifth-order shock-fitting method.

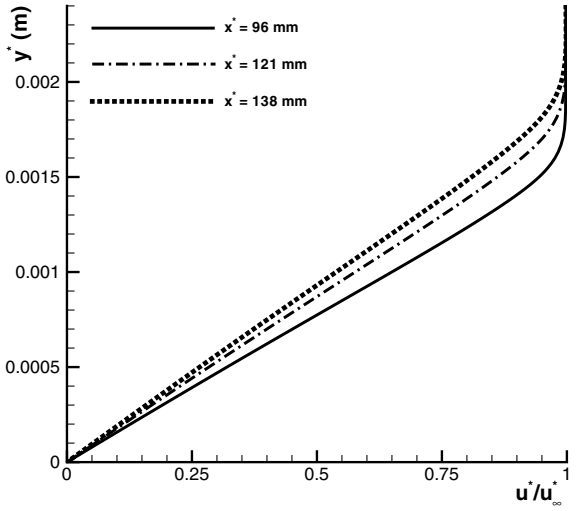

Fig. 5 Distributions of dimensionless streamwise velocity across the boundary layer of the numerical base flow at three different locations.

boundary layer at three different locations. It shows that the thickness of the boundary layer increases with the location shifting downstream. At $x^* = 96$, 121, and 138 mm ($Re = 1134.46$, 1254.19, 1329.66), the thicknesses of the boundary layer are approximately equal to 1.84, 2.04, and 2.20 mm, which has a good agreement with Maslov et al.'s experimental results of about 1.8, 2.0, and 2.2 mm, respectively.

Figures 6 and 7 compare normalized Mach number M/M_∞ and dimensionless streamwise velocity u^*/u^*_∞ distributions across the boundary-layer at three different locations of $x^* = 96$ mm, 121 mm, and 138 mm. In these figures, η is defined as $\eta = y^*/L^*$. The solid lines represent distributions of M/M_∞ and u^*/u^*_∞ obtained by solving the compressible boundary-layer equations. Because of the fact that the solution of boundary-layer equations is self-similar, the distributions of M/M_∞ and u^*/u^*_∞ at different locations are exactly the same for the boundary-layer solution. The unfilled symbols represent experimental results of Maslov et al. [5], whereas the other three lines stand for numerical results simulated by the shock-fitting method. The good agreement between the simulation results indicate that an approximate gradientless flow is obtained over the flat plate, which is evaluated in Maslov et al.'s paper by comparing the experimental results. Figures 6 and 7 show that the numerical results agree well with the experimental results and the boundary-layer solution near the plate. However, in the region of $\eta > 5$, the numerical results have a better agreement with the experimental results. The difference between the numerical results and the boundary-layer solution is mainly caused by viscous–inviscid interaction, because the effect of the bow shock is neglected in the calculation of the compressible boundary-layer equations. The analysis of Figs. 5–7 indicates that the fifth-order shock-fitting method is accurate to simulate the hypersonic flow considered in the current study.

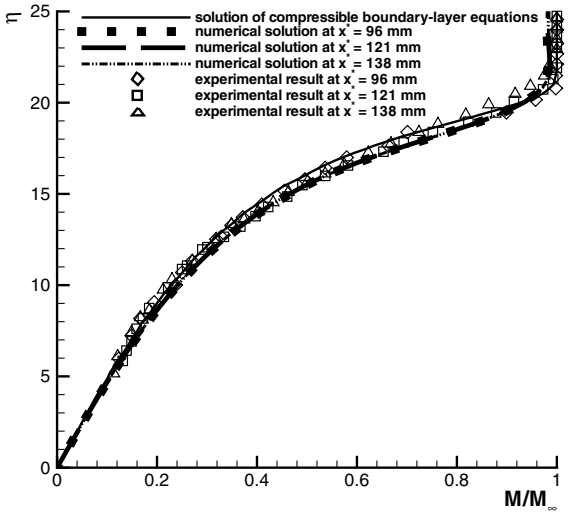

Fig. 6 Comparison of normalized Mach number distributions across the boundary layer at three different locations.

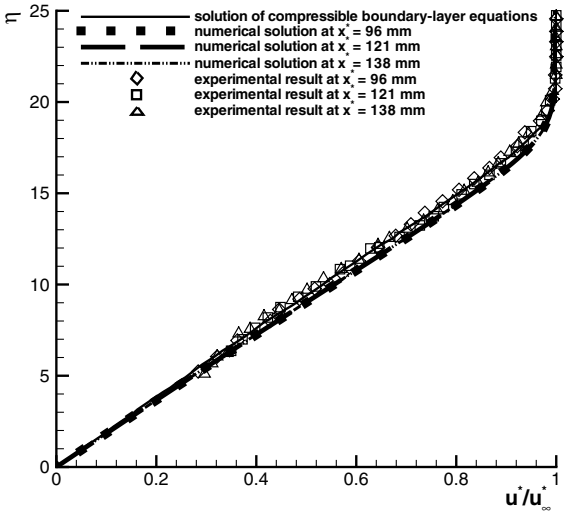

Fig. 7 Comparison of dimensionless streamwise velocity distributions across the boundary layer at three different locations.

B. Receptivity to Three-Dimensional Small Surface Roughness

In compressible boundary layers, Tumin and Reshotko [40] used energy norm to measure the strength of transient growth. The energy norm was defined as

$$E_k = (\mathbf{q}, \mathbf{q})_2 = \int_0^\infty \mathbf{q}^T M \mathbf{q}\, \mathrm{d}y \tag{20}$$

where the perturbation amplitude vector $\mathbf{q}$ and the diagonal matrix M are expressed as

$$\mathbf{q} = (\hat{u}, \hat{v}, \hat{\rho}, \hat{T}, \hat{w})^T \tag{21}$$

$$M = \mathrm{diag}\{\rho, \rho, T/(\gamma\rho Me^2), \rho/[\gamma(\gamma-1)TMe^2], \rho\} \tag{22}$$

In the current paper, the same energy norm is used to evaluate the transient growth. The integral in Eq. (20) is numerically calculated across the boundary layer using a midpoint rule.

For receptivity simulations, boundary conditions of temperature and velocities on a rough surface are linearly transferred to the original smooth surface according to Eqs. (14) and (16). To evaluate the linear extrapolation, numerical simulations are carried out on different height surface roughness. Tables 1 and 2 list the heights of roughness elements with the spanwise wave number β being 0.3021 and 0.1511, respectively. The spanwise wave number β is nondimensionalized by Blasius boundary-layer thickness at the center of the roughness element as

$$\beta = \beta^* L^* \tag{23}$$

Specifically, seven cases of numerical simulations on different height roughness are considered for $\beta = 0.3021$, whereas four cases of numerical simulations on different height roughness are considered for $\beta = 0.1511$. In these two tables, the dimensional heights are nondimensionalized by Blasius boundary-layer thickness at the center of roughness element, that is, $x^* = 4.28125$ mm.

Table 1 Heights of surface roughness with the spanwise wave number being 0.3021 for the seven cases of numerical simulations

n	ϵ	Dimensional height, m	Dimensionless height
1	1.0×10^{-6}	1.0×10^{-6}	0.05785
2	3.0×10^{-6}	3.0×10^{-6}	0.17355
3	5.0×10^{-6}	5.0×10^{-6}	0.28925
4	8.0×10^{-6}	8.0×10^{-6}	0.46280
5	1.0×10^{-5}	1.0×10^{-5}	0.57850
6	5.0×10^{-5}	5.0×10^{-5}	2.89251
7	1.0×10^{-4}	1.0×10^{-4}	5.78502

Table 2 Heights of surface roughness with the spanwise wave number being 0.1511 for the four cases of numerical simulations

n	ϵ	Dimensional height, m	Dimensionless height
1	1.0×10^{-6}	1.0×10^{-6}	0.05785
2	1.0×10^{-5}	1.0×10^{-5}	0.57850
3	5.0×10^{-5}	5.0×10^{-5}	2.89251
4	1.0×10^{-4}	1.0×10^{-4}	5.78502

If linear boundary condition transfer is valid, the perturbation variables are linear to roughness height, and the energy norm in Eq. (20) is proportional to the square of roughness height. Figure 8 compares the energy norms for the seven cases of numerical simulations on different height roughness with the spanwise wave number being 0.3021. Furthermore, Fig. 9 compares the energy norms for the four cases of numerical simulations on different height roughness with the spanwise wave number being 0.1511. In each figure, the energy norm plotted by circular symbols is equal to the product of the original norm for the case of "height $= 1 \times 10^{-6}$ m" and the square of roughness height ratio (>1) between the two cases. For example, in Fig. 8a, the ratio of roughness height between the two cases is three, the energy norm plotted by circular symbols is 9 times the original norm for the case of height $= 1 \times 10^{-6}$ m. The good agreements between the two sets of energy norms in Figs. 8a–8d indicate that the linear extrapolation of the boundary condition is valid for roughness height up to 1×10^{-5} m. Nonlinear effect becomes important when surface roughness is higher than

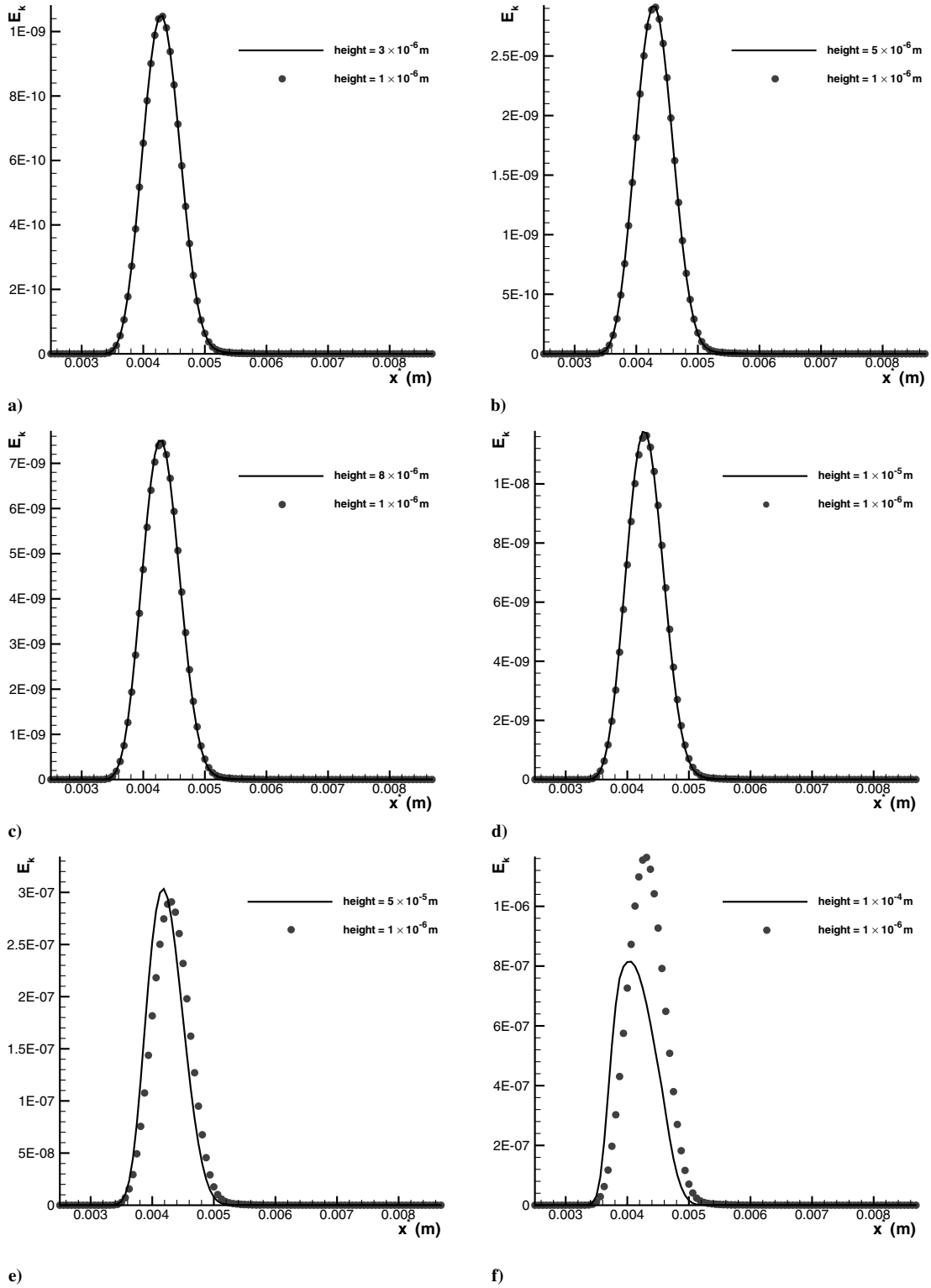

Fig. 8 Energy norm comparisons for the seven cases of numerical simulations on different height roughness with the spanwise wave number being 0.3021.

1×10^{-5} m. The corresponding limitation of dimensionless roughness height for surface roughness is equal to 0.57850, as listed in Table 1. In Fig. 9a, the ratio of roughness height between the two cases is 10, the energy norm plotted by circular symbols is 100 times the original norm for the case of height $= 1 \times 10^{-6}$ m. The agreement between the two sets of energy norms in Fig. 9a indicates that the linear extrapolation of the boundary condition is valid for a roughness height of 1×10^{-5} m. Such results prove that the technique of linear boundary condition transfer is valid as long as the height of surface roughness is smaller than 1×10^{-5} m, approximately $\frac{1}{35}$ of the boundary-layer thickness. In the current study, the height of surface roughness is chosen to be 1×10^{-6} m.

To study the transient growth induced by surface roughness, one case of the receptivity of the hypersonic boundary layer to surface roughness is investigated. For this case, the parameters of surface roughness are as follows:

$$\epsilon = 1.0 \times 10^{-6} \quad \text{and} \quad \beta^* = 1.7355 \times 10^4 \text{ m}^{-1} \tag{24}$$

The dimensional wave number can be nondimensionalized by Blasius boundary-layer thickness at the center of the roughness element as

$$\beta = \beta^* L^* = 0.3021 \tag{25}$$

Figure 10 plots the vector of w' and v' perturbations in the (y^*, z^*) plane at a location of $x^* = 5.4375$ mm ($Re = 277.14$), 0.1875 mm downstream of the trailing edge of the roughness element. It clearly shows that there is a pair of counter-rotating streamwise vortices induced by the surface roughness. Figure 11 shows energy norm distribution along the flat plate. It is noticed that the energy norm only has a small growth in the wake at the location of $x^* = 0.028$ m. The small energy norm increase may be caused by the small height of

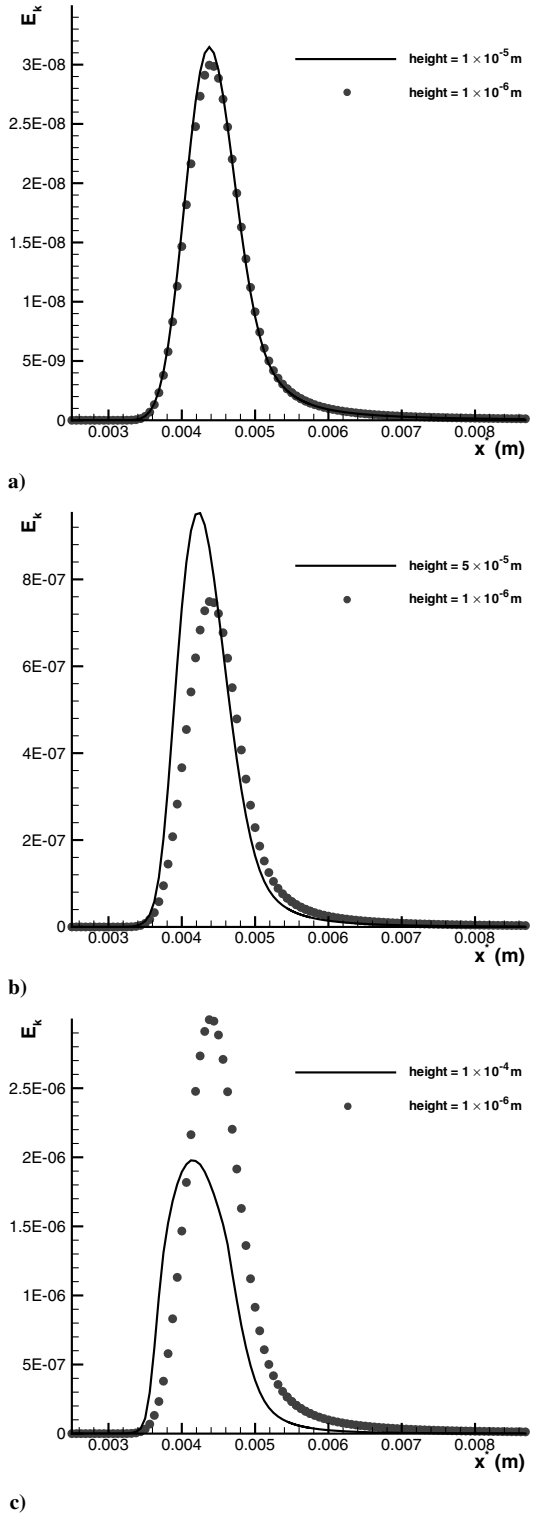

Fig. 9 Energy norm comparisons for the four cases of numerical simulations on different height roughness with the spanwise wave number being 0.1511.

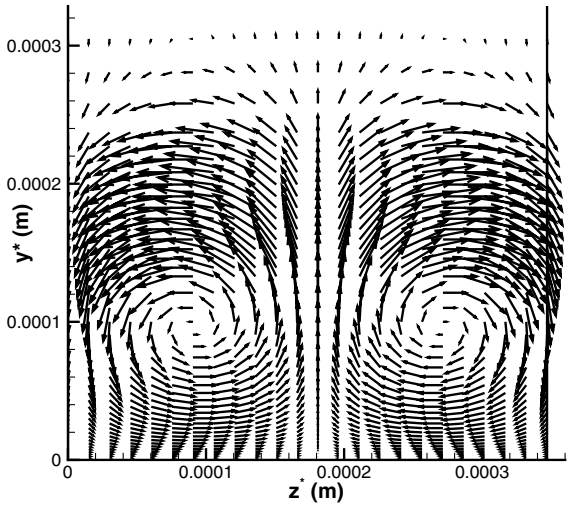

Fig. 10 Vector plot of w' and v' perturbations in the (y^*, z^*) plane at the location of $x^* = 5.4375$ mm for the case of surface roughness with $\beta = 0.3021$.

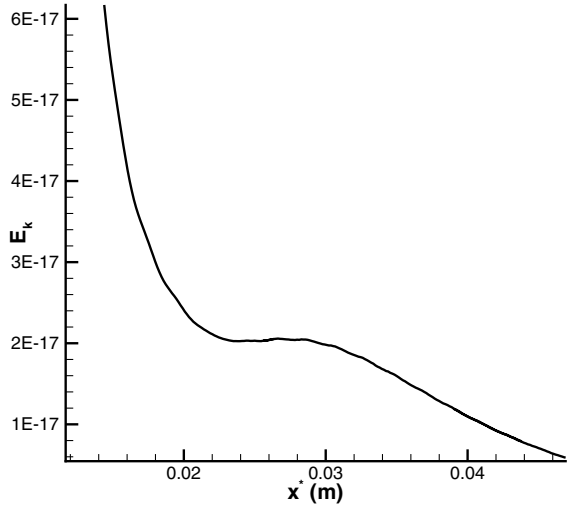

Fig. 11 Energy norm distribution along the flat plate for the case of surface roughness with $\beta = 0.3021$.

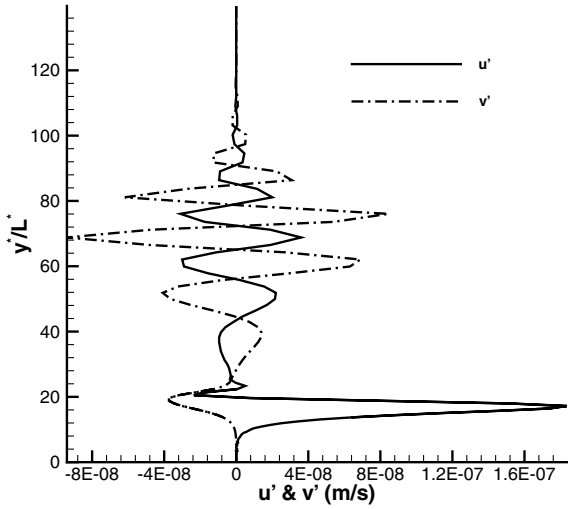

Fig. 12 Streamwise and wall-normal velocity perturbations in wall-normal direction at the location of $x^* = 0.028$ m.

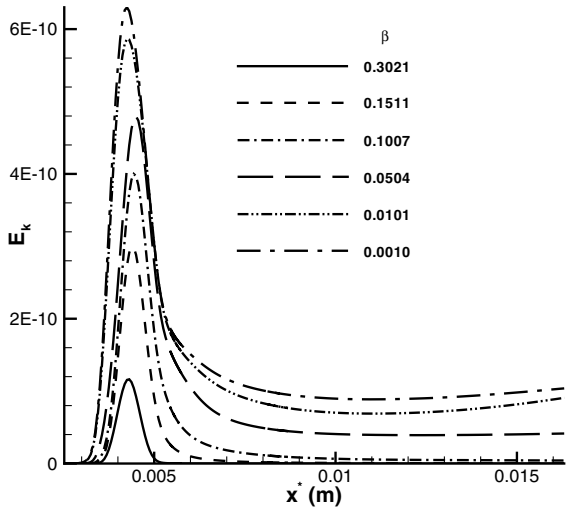

Fig. 13 Energy norm distributions along the flat plate near the roughness element for the six cases of surface roughness with different spanwise wave numbers.

surface roughness. Figure 12 shows the distributions of streamwise and wall-normal velocity perturbations in the wall-normal direction at the location of $x^* = 0.028$ mm. The strong oscillations of velocity perturbations outside the boundary layer ($40 < y^*/L^* < 100$) are related to the acoustic waves propagating along the Mach lines. Profiles of the two velocity perturbations in the boundary layer indicate the existence of vorticity modes in the boundary layer, which is shown in Fig. 10. With the streamwise vortices, momentum transfers from inviscid outer flow to the boundary layer, increases the momentum in the boundary layer. Correspondingly, the energy norm of the disturbance increases, which stands for transient growth.

According to transient growth theory, the maximum energy norm depends on the parameters of disturbances. We do not know which spanwise wave number corresponds to the optimal disturbance. To achieve maximum transient growth, a range of spanwise wave numbers is covered. In the current paper, six cases of surface roughness with different spanwise wave numbers are considered. For all cases, the height of roughness is fixed to 1×10^{-6} m. Table 3 lists the spanwise wave numbers of surface roughness for the six cases, where the dimensional spanwise wave numbers are nondimensionalized by Blasius boundary-layer thickness at the center of roughness element ($x^* = 4.28125$ mm). Figure 13 compares energy norm distributions along the flat plate near the roughness element for the six cases of surface roughness with different spanwise wave numbers. It shows the initial energy norm increases with the increase of the spanwise wave number. In our simulations, surface roughness with even higher spanwise wave numbers has been tested. However, they are not included in current paper, because the initial energy norm for even higher spanwise wave numbers is quite similar to that of $\beta = 0.0010$. Figure 14 compares energy norm distributions along the flat plate further downstream of the roughness element for the six cases of surface roughness with different spanwise wave numbers. It shows that the energy norm initially increases with the increase of the spanwise wave number, however, the energy norm of the case with $\beta = 0.0010$ is smaller than that of the case with $\beta = 0.0101$. Both Figs. 13 and 14 show that the spanwise wave number has a strong effect on transient growth. For the six cases considered in the current

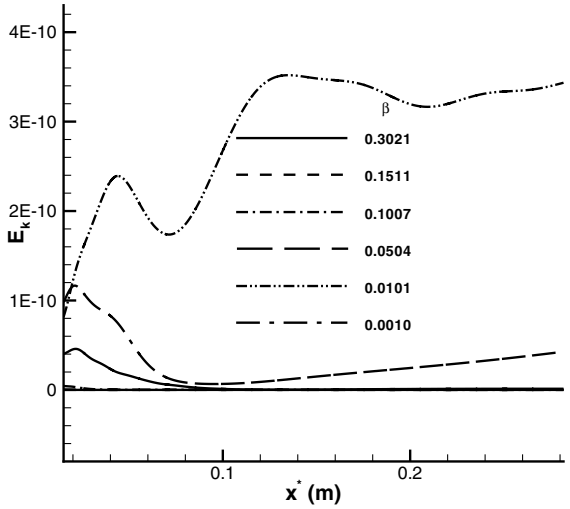

Fig. 14 Energy norm distributions along the flat plate further downstream of the roughness element for the six cases of surface roughness with different spanwise wave numbers.

study, surface roughness with the spanwise wave number being 0.0101 has the strongest excitation of transient growth.

To summarize, the numerical results show that streamwise vortices are induced by surface roughness. Surface roughness with the spanwise wave number being 0.0101 has the strongest excitation of transient growth. In the current study, all numerical simulations are carefully configured and the accuracy of numerical steady base flow has been validated by comparisons with Maslov et al.'s [5] experimental measurements. The results of receptivity simulations are reliable. However, numerical results do not show very strong transient growth, which may be due to the small height of surface

Table 3 Spanwise wave numbers of surface roughness for the six cases of receptivity simulations

n	Dimensional spanwise wave number, m^{-1}	Dimensionless spanwise wave number
1	1.73550×10^4	0.3021
2	8.67752×10^3	0.1511
3	5.78502×10^3	0.1007
4	2.89251×10^3	0.0504
5	5.78502×10^2	0.0101
6	57.85016	0.0010

roughness. The strong transient growth reported in previous experimental studies [19,20,22] was induced by finite height roughness.

V. Conclusions

The receptivity of a hypersonic flat-plate boundary layer to three-dimensional surface roughness is investigated by a series of numerical simulations. The freestream flow conditions are the same as those of Maslov et al.'s leading-edge receptivity experiment [5]. The accuracy of the numerical steady base flow is validated by comparisons with the theoretical self-similar boundary-layer solution and Maslov et al.'s experimental measurements. In receptivity simulations, small surface roughness, periodic in the spanwise direction, is introduced on the flat plate. The subsequent responses of the hypersonic boundary layer are simulated by solving three-dimensional Navier–Stokes equations with a fifth-order shock-fitting method and a Fourier collocation method. Because of the small height of surface roughness, boundary conditions of temperature and velocities on the rough surface are transferred to the original smooth surface by linear extrapolation. The technique of linear boundary condition transfer is proved to be valid as long as the height of surface roughness is smaller than approximately $\frac{1}{35}$ of the boundary-layer thickness. The effect of spanwise wave number on the receptivity is studied by considering six cases of receptivity simulations. The numerical results show that counter-rotating streamwise vortices and transient growth are induced by surface roughness. The spanwise wave number has a strong effect on the excitation of transient growth. For the six cases considered in the current study, surface roughness with the spanwise wave number being 0.0101 has the strongest excitation of transient growth. In the current study, no very strong transient growth is induced by surface roughness, which may be due to the small height of surface roughness.

Acknowledgments

This work was sponsored by the U.S. Air Force Office of Scientific Research under Grant Nos. FA9550-04-1-0029 and FA9550-07-1-0414, monitored by John Schmisseur. The views and conclusions contained herein are those of the authors and should not be interpreted as necessarily representing the official policies or endorsements, either expressed or implied, of the U.S. Air Force Office of Scientific Research or the U.S. Government.

References

[1] Lees, L., and Lin, C. C., "Investigation of the Stability of the Laminar Boundary Layer in Compressible Fluid," NACA TN 1115, 1946.

[2] Mack, L. M., "Linear Stability Theory and the Problem of Supersonic Boundary-Layer Transition," *AIAA Journal*, Vol. 13, No. 3, 1975, pp. 278–289. doi:10.2514/3.49693

[3] Kendall, J. M., "Wind Tunnel Experiments Relating to Supersonic and Hypersonic Boundary-Layer Transition," *AIAA Journal*, Vol. 13, No. 3, 1975, pp. 290–299. doi:10.2514/3.49694

[4] Malik, M. R., Lin, R. S., and Sengupta, R., "Computation of Hypersonic Boundary-Layer Response to External Disturbances," AIAA Paper 1999-0411, Jan. 1999.

[5] Maslov, A. A., Shiplyuk, A. N., Sidorenko, A., and Arnal, D., "Leading-Edge Receptivity of a Hypersonic Boundary Layer on a Flat Plate," *Journal of Fluid Mechanics*, Vol. 426, Jan. 2001, pp. 73–94. doi:10.1017/S0022112000002147

[6] Saric,W. S., Reed, H. L., and Kerschen, E. J., "Boundary-Layer Receptivity to Freestream Disturbances," *Annual Review of Fluid Mechanics*, Vol. 34, Jan. 2002, pp. 291–319. doi:10.1146/annurev.fluid.34.082701.161921

[7] Reshotko, E., "Is Re_θ/Me a Meaningful Transition Criterion?," AIAA Paper 2007-0943, Jan. 2007.

[8] Goldstein, M. E., and Hultgren, L. S., "Boundary-Layer Receptivity to Long-Wave Freestream Disturbances," *Annual Review of Fluid Mechanics*, Vol. 21, Jan. 1989, pp. 137–166. doi:10.1146/annurev.fl.21.010189.001033

[9] Fedorov, A. V., and Khokhlov, A. P., "Receptivity of Hypersonic Boundary Layer to Wall Disturbances," *Theoretical and Computational Fluid Dynamics*, Vol. 15, No. 4, 2002, pp. 231–254. doi:10.1007/s001620100052

[10] Tumin, A., Wang, X., and Zhong, X., "Direct Numerical Simulation and the Theory of Receptivity in a Hypersonic Boundary Layer," *Physics of Fluids*, Vol. 19, No. 1, Jan. 2007, p. 014101. doi:10.1063/1.2409731

[11] Ma, Y., and Zhong, X., "Receptivity of a Supersonic Boundary Layer over a Flat Plate, Part 1: Wave Structures and Interactions," *Journal of Fluid Mechanics*, Vol. 488, July 2003, pp. 31–78. doi:10.1017/S0022112003004786

[12] Ma, Y., and Zhong, X., "Receptivity of a Supersonic Boundary Layer over a Flat Plate, Part 2: Receptivity to Freestream Sound," *Journal of Fluid Mechanics*, Vol. 488, July 2003, pp. 79–121. doi:10.1017/S0022112003004798

[13] Bertolotti, F. P., "Vortex Generation and Wave-Vortex Interaction over a Concave Plate with Roughness and Suction," Inst. for Computer Applications in Science and Engineering Rept. No. 93-101, 1993.

[14] Choudhari, M., "Roughness-Induced Generation of Crossflow Vortices in Three-Dimensional Boundary Layers," *Theoretical and Computational Fluid Dynamics*, Vol. 6, No. 1, 1994, pp. 1–30. doi:10.1007/BF00417924

[15] Hanifi, A., Schmid, P. J., and Henningson, D. S., "Transient Growth in Compressible Boundary Layer Flow," *Physics of Fluids*, Vol. 8, No. 3, 1996, pp. 826–837. doi:10.1063/1.868864

[16] Andersson, P., Berggren, M., and Henningson, D. S., "Optimal Disturbances and Bypass Transition in Boundary Layers," *Physics of Fluids*, Vol. 11, No. 1, 1999, pp. 134–150. doi:10.1063/1.869908

[17] Tumin, A., "Receptivity of Compressible Boundary Layers to Three-Dimensional Wall Perturbations," AIAA Paper 2006-1110, Jan. 2006.

[18] Maslov, A. A., and Semenov, N. V., "Excitation of Natural Oscillations in a Boundary Layer by an External Acoustic Field," *Fluid Dynamics* (Historical Archive), Vol. 21, No. 3, May 1986, pp. 400–404. doi:10.1007/BF01409724

[19] White, E. B., "Transient Growth of Stationary Disturbances in a Flat Plate Boundary Layer," *Physics of Fluids*, Vol. 14, No. 12, 2002, pp. 4429–4439. doi:10.1063/1.1521124

[20] White, E. B., and Ergin, F. G., "Receptivity and Transient Growth of Roughness-Induced Disturbances," AIAA Paper 2003-4243, June 2003.

[21] Fransson, J. H. M., and Brandt, L., "Experimental and Theoretical Investigation of the Nonmodal Growth of Steady Streaks in a Flat Plate Boundary Layer," *Physics of Fluids*, Vol. 16, No. 10, 2004, pp. 3627–3638. doi:10.1063/1.1773493

[22] White, E. B., Rice, J. M., and Ergin, F. G., "Receptivity of Stationary Transient Disturbances to Surface Roughness," *Physics of Fluids*, Vol. 17, No. 6, 2005, p. 064109. doi:10.1063/1.1938217

[23] Bottaro, A., and Zebib, A., "Görtler Vortices Promoted by Wall Roughness," *Fluid Dynamics Research*, Vol. 19, No. 6, June 1997, pp. 343–362. doi:10.1016/S0169-5983(96)00055-X

[24] Collis, S. S., and Lele, S. K., "Receptivity to Surface Roughness near a Swept Leading Edge," *Journal of Fluid Mechanics*, Vol. 380, Feb. 1999, pp. 141–168. doi:10.1017/S0022112098003449

[25] Zhong, X., "Leading-Edge Receptivity to Free Stream Disturbance Wave for Hypersonic Flow over a Parabola," *Journal of Fluid Mechanics*, Vol. 441, Aug. 2001, pp. 315–367. doi:10.1017/S0022112001004918

[26] Ma, Y., and Zhong, X., "Receptivity of a Supersonic Boundary Layer over a Flat Plate, Part 3: Effects of Different Types of Free-Stream Disturbances," *Journal of Fluid Mechanics*, Vol. 532, May 2005, pp. 63–109. doi:10.1017/S0022112005003836

[27] Egorov, I. V., Fedorov, A. V., and Soudakov, V. G., "Direct Numerical Simulation of Unstable Disturbances in Supersonic Boundary Layer," AIAA Paper 2004-0588, Jan. 2004.

[28] Fischer, P., and Choudhari, M., "Numerical Simulation of Roughness-Induced Transient Growth in a Laminar Boundary Layer," AIAA Paper 2004-2539, June 2004.

[29] Choudhari, M., and Fischer, P., "Roughness-Induced Transient Growth," AIAA Paper 2005-4765, June 2005.

[30] Wang, X., and Zhong, X., "Receptivity of a Mach 8.0 Flow over a Sharp

Wedge to Wall Blowing-Suction," AIAA Paper 2005-5025, June 2005.
[31] Reshotko, E., and Tumin, A., "Role of Transient Growth in Roughness-Induced Transition," *AIAA Journal*, Vol. 42, No. 4, 2004, pp. 766–770. doi:10.2514/1.9558
[32] Zhong, X., "High-Order Finite-Difference Schemes for Numerical Simulation of Hypersonic Boundary-Layer Transition," *Journal of Computational Physics*, Vol. 144, No. 2, Aug. 1998, pp. 662–709. doi:10.1006/jcph.1998.6010
[33] Zhong, X., and Lee, T., "Nonequilibrium Real-Gas Effects on Disturbance/Bow Shock Interaction in Hypersonic Flow past a Cylinder," AIAA Paper 1996-1856, Jan. 1996.
[34] Ma, Y., and Zhong, X., "Receptivity to Freestream Disturbances of Mach 8 Flow over a Sharp Wedge," AIAA Paper 2003-0788, 2003.
[35] Tumin, A., Wang, X., and Zhong, X., "Direct Numerical Simulation of Receptivity in a Hypersonic Boundary Layer: Validation," AIAA Paper 2006-1108, Jan. 2006.
[36] Zhong, X., "Receptivity of Mach 6 Flow over a Flared Cone to Freestream Disturbance," AIAA Paper 2004-0253, Jan. 2004.
[37] Wang, X., and Zhong, X., "Numerical Simulation of Hypersonic Boundary-Layer Receptivity to Two- and Three-Dimensional Wall Perturbations," AIAA Paper 2007-0946, Jan. 2007.
[38] Ma, Y., and Zhong, X., "Receptivity to Freestream Disturbances of Mach 4.5 Flow over a Flat Plate," AIAA Paper 2002-0140, Jan. 2002.
[39] Wang, X., and Zhong, X., "Numerical Simulation and Experiment Comparison of Leading-Edge Receptivity of a Mach 5.92 Boundary Layer," AIAA Paper 2006-1107, Jan. 2006.
[40] Tumin, A., and Reshotko, E., "Spatial Theory of Optimal Disturbances in Boundary Layers," *Physics of Fluids*, Vol. 13, No. 7, 2001, p. 2097. doi:10.1063/1.1378070

R. Kimmel
Associate Editor